Biomaterials 32 (2011) 3520–3537

Contents lists available at ScienceDirect

Biomaterials

journal homepage: www.elsevier.com/locate/biomaterials

Intracellular delivery of quantum dots mediated by a histidine- and arginine-rich HR9 cell-penetrating peptide through the direct membrane translocation mechanism

Betty R. Liu [a,b], Yue-wern Huang [c,**], Jeffrey G. Winiarz [d], Huey-Jenn Chiang [b], Han-Jung Lee [a,*]

[a] Department of Natural Resources and Environmental Studies, National Dong Hwa University, No. 1, Sec. 2, Da-Hsueh Road, Shoufeng, Hualien 97401, Taiwan
[b] Graduate Institute of Biotechnology, National Dong Hwa University, No. 1, Sec. 2, Da-Hsueh Road, Shoufeng, Hualien 97401, Taiwan
[c] Department of Biological Sciences, Missouri University of Science and Technology, 105 Schrenk Hall, 400 West 11th Street, Rolla, MO 65409-1120, USA
[d] Department of Chemistry, Missouri University of Science and Technology, 142 Schrenk Hall, 400 West 11th Street, Rolla, MO 65409-1120, USA

ARTICLE INFO

Article history:
Received 31 December 2010
Accepted 13 January 2011
Available online 16 February 2011

Keywords:
Cell-penetrating peptides (CPPs)
Cellular internalization
Protein transduction domains (PTDs)
Quantum dots (QDs)
Semiconductor

ABSTRACT

Functional peptides that transfer biomaterials, such as semiconductor quantum dots (QDs), into cells in biomaterial research have been developed in recent years. Delivery of QDs conjugated with cell-penetrating peptides (CPPs) into cells by the endocytic pathway was problematic in biomedical applications because of lysosomal trapping. Here, we demonstrate that histidine- and arginine-rich CPPs (HR9 peptides) stably and noncovalently combined with QDs are able to enter into cells in an extremely short period (4 min). Interrupting both F-actin polymerization and active transport did not inhibit the entry of HR9/QD complexes into cells, indicating that HR9 penetrates cell membrane directly. Subcellular colocalization studies indicated that QDs delivered by HR9 stay in cytosol without any organelle capture. Dimethyl sulphoxide, ethanol and oleic acid, but not pyrenebutyrate, enhanced HR9-mediated intracellular delivery of QDs by promoting the direct membrane translocation pathway. HR9 and HR9/QDs were not cytotoxic. These findings suggest that HR9 could be an efficient carrier to deliver drugs without interfering with their therapeutic activity.

1. Introduction

The internalization of exogenous materials through plasma membranes by endocytosis is a vital function of eukaryotic cells [1]. Endocytosis involves formation of vesicles that later fuse with endosomes. The contents from endocytosis usually enter the endo-lysosomal system and are digested in acid hydrolases-containing lysosomes [2]. While this trafficking process is indispensable for nutrient internalization, self-protection from toxins and presentation of antigens [1], it limits the efficient delivery of pharmaceuticals and other biologically active molecules by this pathway, as they will become entrapped and degraded in the acidic endosomal environment.

Several intracellular drug delivery systems have been developed, each of which possess certain intrinsic limitations [3,4]. Cell-penetrating peptides (CPPs), also called protein transduction domains (PTDs) or arginine-rich intracellular delivery (AID) peptides, are a group of short peptides that possess the ability to penetrate cell membrane, and thus have been considered as candidates for mediating drug delivery [5]. CPPs are amphipathic, hydrophobic or cationic peptides [6]. Zorko and Langel categorized CPPs into three classes: protein-derived CPPs, model peptides and designed peptides [7]. Transactivator of transcription (TAT) and penetratin, two peptides derived from specific protein domains, are typical examples of protein-derived CPPs [7]. Model CPPs include sequences that contain repeat motifs or poly-residues, such as MAP (KLAL) peptide and polyarginine [7]. Designed CPPs are chimeric peptides comprised of various functional domains of target proteins. However, the efficiency of protein transduction displayed by these CPPs varies within the same class and among classes. In an alternative approach, the secondary structure of CPPs that interact with artificial membranes has been characterized [8]. The kinetics of cellular internalization varies with the different CPPs [9]. Thus,

Abbreviations: AID, arginine-rich intracellular delivery; BFP, blue fluorescent protein; CPP, cell-penetrating peptide; CytD, cytochalasin D; DMSO, dimethyl sulphoxide; GFP, green fluorescent protein; HR9, histidine-rich nona-arginine; LDH, lactate dehydrogenase; OA, oleic acid; PB, pyrenebutyrate; PR9, Pas nona-arginine; RFP, red fluorescent protein; PTD, protein transduction domain; QD, quantum dot; R8, octa-arginine; R9, nona-arginine; SR9, synthetic nona-arginine; SRB, sulforhodamine B.

* Corresponding author. Tel.: +886 3 8633642; fax: +886 3 8633260.
** Corresponding author. Tel.: +1 573 341 6589; fax: +1 573 341 4821.
E-mail addresses: huangy@mst.edu (Y.-w. Huang), hjlee@mail.ndhu.edu.tw (H.-J. Lee).

0142-9612/$ – see front matter © 2011 Elsevier Ltd. All rights reserved.
doi:10.1016/j.biomaterials.2011.01.041

CPPs can be clustered into different subgroups based on both the secondary structure and kinetics of CPPs by a functionality-based categorization [9].

CPPs are powerful penetrating biomaterials that are able to deliver bioactive macromolecules (cargoes) such as proteins, nucleic acids, peptide nucleic acids, inorganic particles and liposomes into cells of various species [10–16]. The size of cargoes can be as large as 200 nm in diameter [16]. The concentration of CPPs required in biological applications can be up to 100 μM without causing any cellular injury [17]. Accordingly, the CPP-mediated delivery systems have several desirable characteristics for a drug delivery system: large capacity, high transduction efficiency, rapid transduction rate and very low cytotoxicity.

Fluorescent proteins have been used as probes for imaging and tracking in biomedical applications. However, they have intrinsic disadvantages, including easy bleaching, un-tunable emission wavelength and broad emission range. These limit their use for long-term and multiplex monitoring. Quantum dots (QDs), inorganic semiconductor nanoparticles, have emerged as alternatives to traditional fluorescent proteins. Advantages of QDs include size- and composition-tunable emission with wide excitation and narrow emission spectral ranges, photostability, resistance to photobleaching and chemical degradation, as well as high levels of brightness [18,19]. Accordingly, QDs are being used more frequently for studies of living cells. However, QDs alone do not readily enter cells, and aggregation often occurs after internalization [19,20]. To overcome these limitations, surface modified QDs functionalized by covalent [21–23] or noncovalent [15,24,25] linkages with CPPs, denoted as CPP-QDs or CPP/QDs respectively, have been introduced recently.

The routes of entry and intracellular transport mechanism employed influence the destination and biological efficacy of intracellularly delivered therapeutic agents. The internalization mechanisms used by CPPs and CPP/QDs are incompletely understood. Several studies have demonstrated that the pathways of QDs internalization depended on their conjugated peptides or carriers [26–28]. Two major routes for CPPs to enter cells have been documented: the endocytosis-mediated pathway and direct membrane translocation (also called the pore-opening mechanism) [29]. The former is further divided into three subtypes depending on the cellular molecules involved. For instance, Kawamura et al. demonstrated that p53-TAT fused CPPs enter Chinese hamster ovary cells via clathrin-dependent endocytosis [30]. In contrast, the caveolae-dependent pathway was utilized by CPPs crosslinked with cargoes [31,32]. Actin-dependent macropinocytosis, a nonclassical endocytosis, has recently been proposed in studies with conjugated CPPs [33]. Ruan et al. found that macropinocytosis which involved actin filaments and microtubules was the major route for CPP-QDs uptake and intracellular transport [27]. In our recent studies, CPPs were found to enter into cells in covalent and noncovalent protein transduction (CNPT) manners that involved multiple pathways [34,35]. All of these studies support the notion that both cargoes and conjugation strategies influence the route of cellular internalization of CPPs.

In drug delivery, molecules entering cells via the direct membrane translocation pathway is preferred, as this route does not incur endosomal entrapment [36]. Several studies have found that arginine-rich CPPs, such as nona-arginine (R9) peptide, destabilized the plasma membrane creating transient pores for cellular penetration [37,38]. CPPs using the direct translocation pathway are capable of passing through membrane barriers, staying in the cytosol or nucleus by avoiding organelle confinement.

Transduction enhancers and endosomolytic agents have been employed to improve transduction efficiency and to overcome endosomal entrapment [39–41]. Most enhancers either increase the net hydrophobicity of CPPs or increase membrane permeability [39,41]. Lo and Wang discovered that a PTD of TAT comprised of additional polyhistidine and cysteine residues possessed endosomolytic properties and increased the gene expression of DNAs carried by this CPP [42]. Takayama et al. reported that a short Pas (FFLIPKG) peptide enhanced the intracellular delivery of octa-arginine within 5 min, even in the presence of serum [43].

Most conjugation methods involve either covalent linkage with thiol groups [21–23] or noncovalent linkage via biotin–streptavidin interactions [15,24,25] between QDs and CPPs. Covalently linking QDs and CPPs is a lengthy process that requires purification and chemical identification. Our studies have demonstrated that noncovalent linking is effective, inexpensive and relatively easy [15,24,25].

In this study, our goals were to 1) compare the transduction efficiency of three R9-containing CPPs that form complexes with QDs in a noncovalent fashion and 2) determine the mechanisms of CPP-mediated uptake and subcellular localization of QDs. To achieve these goals, we first analyzed the noncovalent interactions between CPPs and QDs. We then examined the kinetics of transduction for the three CPPs using live cell imaging and flow cytometry. To elucidate the uptake mechanisms involved, pharmacological and physical inhibitors were applied to block biomolecules mediating the various endocytic pathways. We hypothesized that certain CPPs can internalize QDs by direct membrane translocation. Insofar as 5–15 min is required for endosome formations in case of endocytosis [7,44], we have adopted a strategy in which the direct membrane translocation was measured at 4 min [39]. Organelle-specific markers were utilized to identify the subcellular localization of QDs after delivery by CPPs.

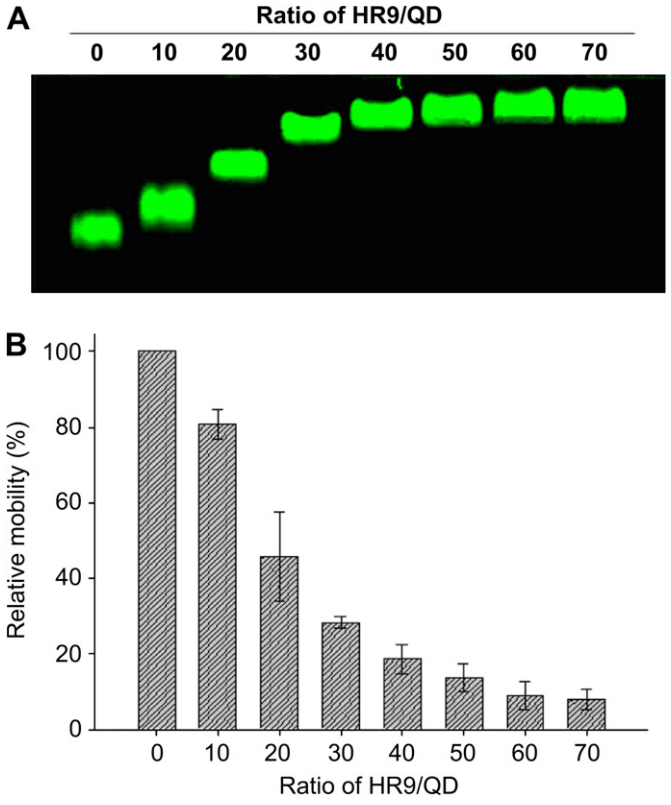

Fig. 1. Noncovalent interactions between HR9 peptides and QDs. A: Gel retardation assay indicating interactions between HR9 and QDs. Different amounts of HR9 were mixed with QDs at molecular ratios of 0 (QD only), 10, 20, 30, 40, 50, 60 and 70. After an oxidative incubation of two cysteine residues becoming a dimeric cystine at 37 °C for 2 h, the mixtures were analyzed by electrophoresis on a 0.5% agarose gel. Fluorescence of QDs was visualized at 473 nm. B: Histogram of the relative mobility of HR9/QD complexes. The mobility of HR9/QDs was determined and converted into a statistic presentation.

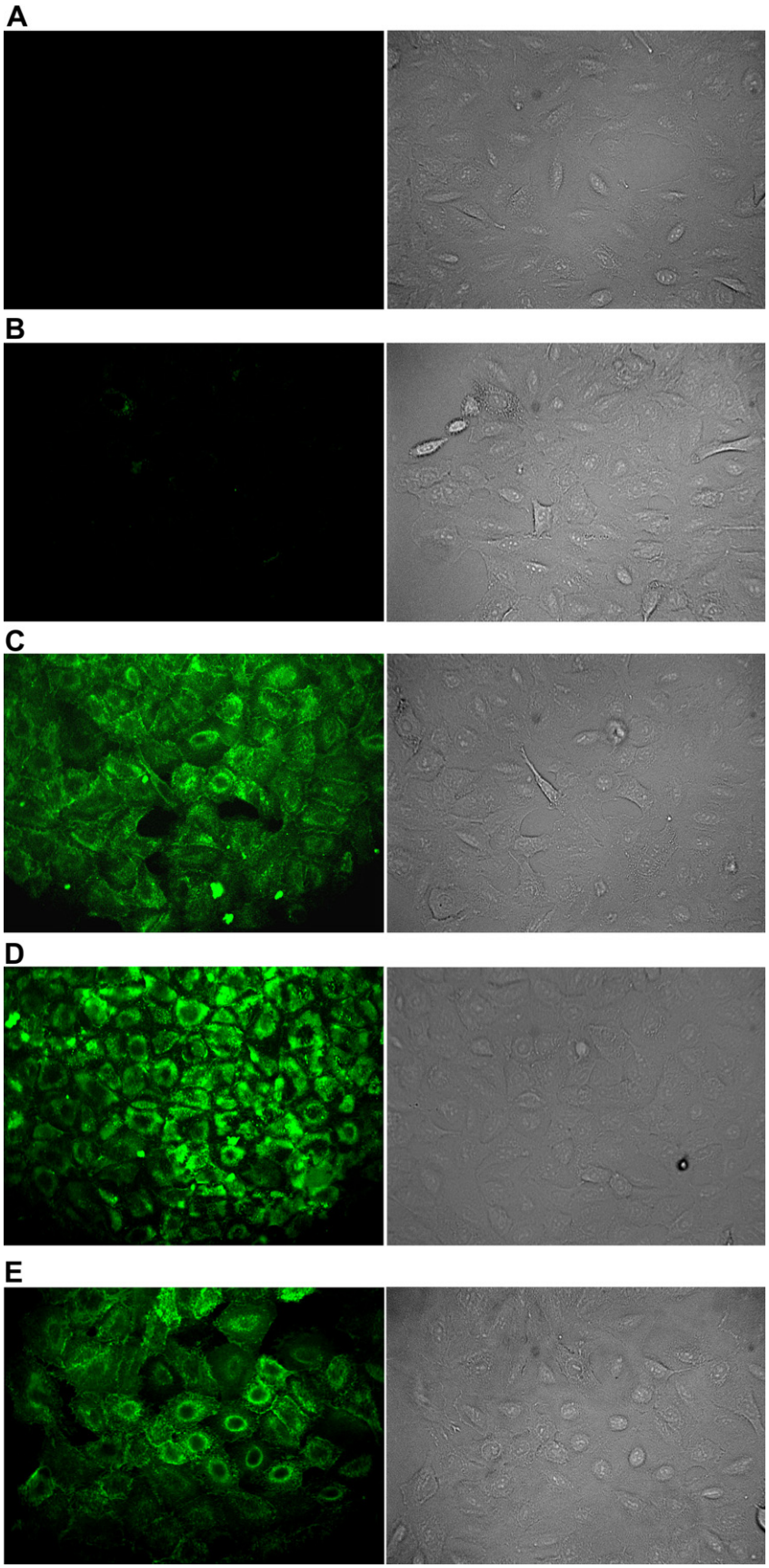

Fig. 2. Confocal microscopy of intracellular delivery of CPP/QD complexes into A549 cells. A: Internal control. Human A549 cells without any treatments were observed under the GFP channel (left column) or transmitted light (right column) at a magnification of 200×. B: Negative control. Cells treated with QDs only for 1 h. C: Positive control. Cells were treated with SR9/QDs (60:1) for 1 h. D: Treatment with HR9/QD (60:1) complexes for 1 h. E: Treatment with PR9/QD (60:1) complexes for 1 h.

2. Materials and methods

2.1. QDs and peptides preparation

CdSe/ZnS quantum dots (carboxyl-functionalized eFluor 525NC) with the maximal emission peak wavelength at 525 nm were purchased from eBioscience (San Diego, CA, USA). Three chemically synthetic arginine-rich CPPs were purchased from MDBio (Taipei, Taiwan): synthetic nona-arginine (SR9) of 86.3% purity, histidine-rich nona-arginine (HR9; C-5H-R9-5H-C) of 87.0% purity and Pas nona-arginine (PR9; FFLIPKG-R9) of 98.9% purity. Various amounts of SR9, HR9 and PR9 peptides were mixed with QDs and incubated at 37 °C for designated periods of time. A molecular ratio between peptides and QDs of 60:1 produced maximal CPP/QD complexes according to gel retardation assays, and this ratio was used in subsequent experiments.

2.2. Gel retardation assay

Various amounts of HR9 were mixed with 2 μM of QDs in phosphate buffered saline (PBS) and incubated at 37 °C for 2 h for an oxidative reaction of two cysteine residues becoming a dimeric cystine. Different molecular ratios of HR9/QDs from 0 to 70 were analyzed by electrophoresis on a 0.5% agarose gel (Multi ABgarsoe, ABgene, UK) in 0.5 × TAE (40 mM of Tris-acetate and 1 mM of EDTA, pH 8.0) buffer at 100 V for 40 min [15]. Images were captured by the Typhoon FLA 9000 biomolecular imager (GE Healthcare, Piscataway, NJ, USA) with the excitation wavelength at 473 nm of LD laser and with the emission above 473 nm by LPB filter. Data were analyzed with the ImageQuant TL 7.0 software (GE Healthcare).

2.3. Cell culture

Human bronchoalveolar carcinoma A549 cells (American Type Culture Collection, Manassas, VA, USA; CCL-185) were cultured in Roswell Park Memorial Institute (RPMI) 1640 medium (Gibco, Invitrogen, Carlsbad, CA, USA) supplemented with 10% (v/v) bovine serum (BS; Gibco) as previously described [15]. In experiments, cells were washed with PBS three times. The culture medium was switched to RPMI 1640 medium supplemented with 1% BS during exposure to CPP/QDs.

2.4. Noncovalent protein transduction

In protein transduction tests, 100 nM of QDs were mixed with 6 μM of SR9, HR9 or PR9 peptides at 37 °C for 2 h, and then incubated with A549 cells for 1 h. In kinetic studies of transduction, cells were treated with CPP/QD mixtures for 0, 4, 10 and 30 min at 37 °C. For inhibition of endocytosis, physical and chemical endocytic modulators were used as follows. For physical inhibition of endocytosis, cells were prepared at 4 °C and then incubated at 4 °C for 30 min in order to deplete energy required by all endocytic pathways. CPP/QDs were added to cells and incubated at 4 °C for 4 min. In drug inhibition studies, cells were treated with 10 μM of cytochalasin D (CytD; Sigma–Aldrich, St. Louis, MO, USA) for 30 min to block F-actin rearrangements followed by the treatment of CPP/QDs for 4 min.

To determine subcellular localization, Hoechst 33342, LysoTracker DND-99, MitoTracker Deep Red FM, Texas Red-X phalloidin, Cellular Lights MAP4-RFP and ER-Tracker Red (Invitrogen) were utilized to visualize nucleus, lysosome, mitochondrium, F-actin, microtubule and endoplasmic reticulum, respectively. Cells were treated with CPP/QDs for 4 min at 37 °C followed by fixation with 3.7% formaldehyde. Cells were stained with fluorescent organelle-specific trackers according to the manufacturer's instructions (Invitrogen).

The influence of chemical enhancers of transduction, such as dimethyl sulphoxide (DMSO), ethanol (EtOH), oleic acid (OA) and pyrenebutyrate (PB) (Sigma–Aldrich) were studied in protein transduction experiments. Cells were pretreated with either 10% DMSO or 1% ethanol in serum-free medium for 1 h [41], and then CPP/QDs were added for an additional 4 min period. Cells were pretreated with 4 or 50 μM of PB for 2 min [39] and then were incubated with either R9-GFP fusion protein or CPP/QDs for an additional 4 min period. Cells were treated with either CPP/QDs containing medium or both CPP/QDs and 80 μM of OA [45] containing medium for 4 min.

2.5. Wound assay

Cells were cultured to be more than 90% confluence, and then starved in 1% serum-containing medium overnight. On the day of the assay, scratching lines were made through cells moving perpendicular to the marker line, and cell debris was removed by rinsing with PBS. Cells were either fixed immediately or recovered in normal culture medium at 37 °C for 24 h. Both Hoechst 33342 and Texas Red-X phalloidin were used according to the manufacturer's instructions (Invitrogen) for the detection of nucleus and F-actin, respectively. Cells were observed and recorded using an inverted TMS microscope (Nikon, Melville, NY, USA) equipped with an MD130 CMOS sensor (Electronic Eyepiece, Dar-An, Taiwan) for morphology in bright-field and with a BD Pathway 435 system (BD Biosciences, Franklin Lakes, NJ, USA) for fluorescent images.

2.6. Fluorescent and confocal microscopy

Fluorescent and bright-field images were recorded using a BD Pathway 435 System (BD Biosciences) with the Olympus UApo/340 20×/0.17 objective and PlanApo N 60×/1.42 oil objective (Olympus, Tokyo, Japan). This system included the fluorescent and confocal microscopic sets. The BD AttoVision and BD IPLab of the BD pathway system were the software packages used to analyze and convert images from 16/48 bits to 8/24 bits. Excitation filters were set at 377/50 nm, 482/35 nm and 543/22 nm for blue, green and red fluorescence, respectively. Emission filters were set at 435LP (long-pass), 536/40 nm and 593/40 nm for blue (BFP), green (GFP) and red fluorescent protein (RFP) channels, respectively. Transmitted light without the excitation filter, but with 536/40 nm emission filter, was used to observe cell morphology as bright-field images.

2.7. Flow cytometric analysis

Human A549 cells were seeded in 24-well plates. Cells in the control and the experimental groups were harvested and analyzed using a flow cytometer, as previously described [11].

2.8. Cytotoxicity measurement

In cytotoxicity assays, cells were treated with 6 μM of CPPs, 100 nM of QDs or CPP/QDs for 24 h at 37 °C. Cells without any treatments served as the negative control, while cells treated with DMSO served as the positive control. A sulforhodamine B (SRB) colorimetric assay was performed as previously described [15,34].

2.9. Statistical analysis

Data are presented as mean ± standard deviations (SDs). Statistical comparisons between the control and experimental groups were performed using the Student's *t*-test. Mean values and SDs were calculated for each sample examined in at least triplicate independent experiments. The level of statistical significance was set at $P < 0.05$ (*, †) or 0.01 (**, ††).

3. Results

A gel retardation assay was used to confirm interactions between arginine-rich CPPs and QDs. HR9 peptides were mixed and incubated with carboxylated QDs in different ratios. Our results indicated that HR9 indeed interacted with QDs noncovalently, and the shifts of HR9/QD complexes depended on the amount of HR9 added (Fig. 1A). Statistical analysis revealed that the relative mobility decreased when the ratio of HR9/QDs increased (Fig. 1B). The mobility of complexes was optimal at ratios of 60 and 70 (Fig. 1), accordingly, and we used 60 as the combination ratio in subsequent experiments.

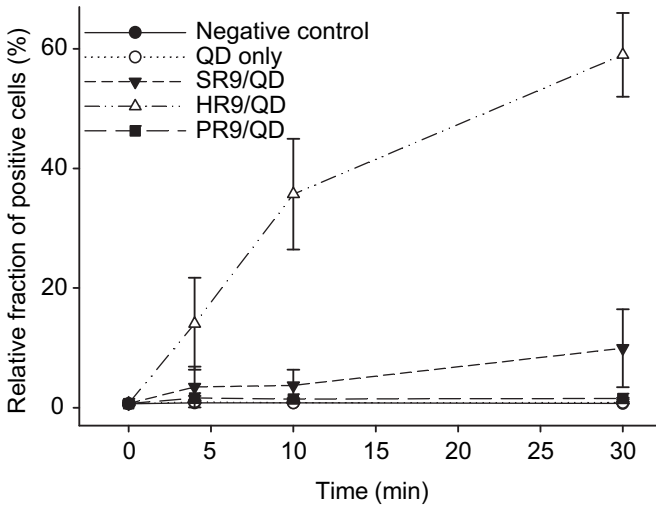

Fig. 3. Kinetics of the cellular internalization of CPP/QD complexes. Cells were treated with QDs only, SR9/QDs, HR9/QDs or PR9/QDs for designated period of time (0, 4, 10 and 30 min). The molecular ratio between CPPs and QDs was 60:1. Cells without any treatments were served as the negative control. The fluorescent intensity was analyzed using a flow cytometer. Data are presented as mean ± SD from 7 independent experiments in each treatment group.

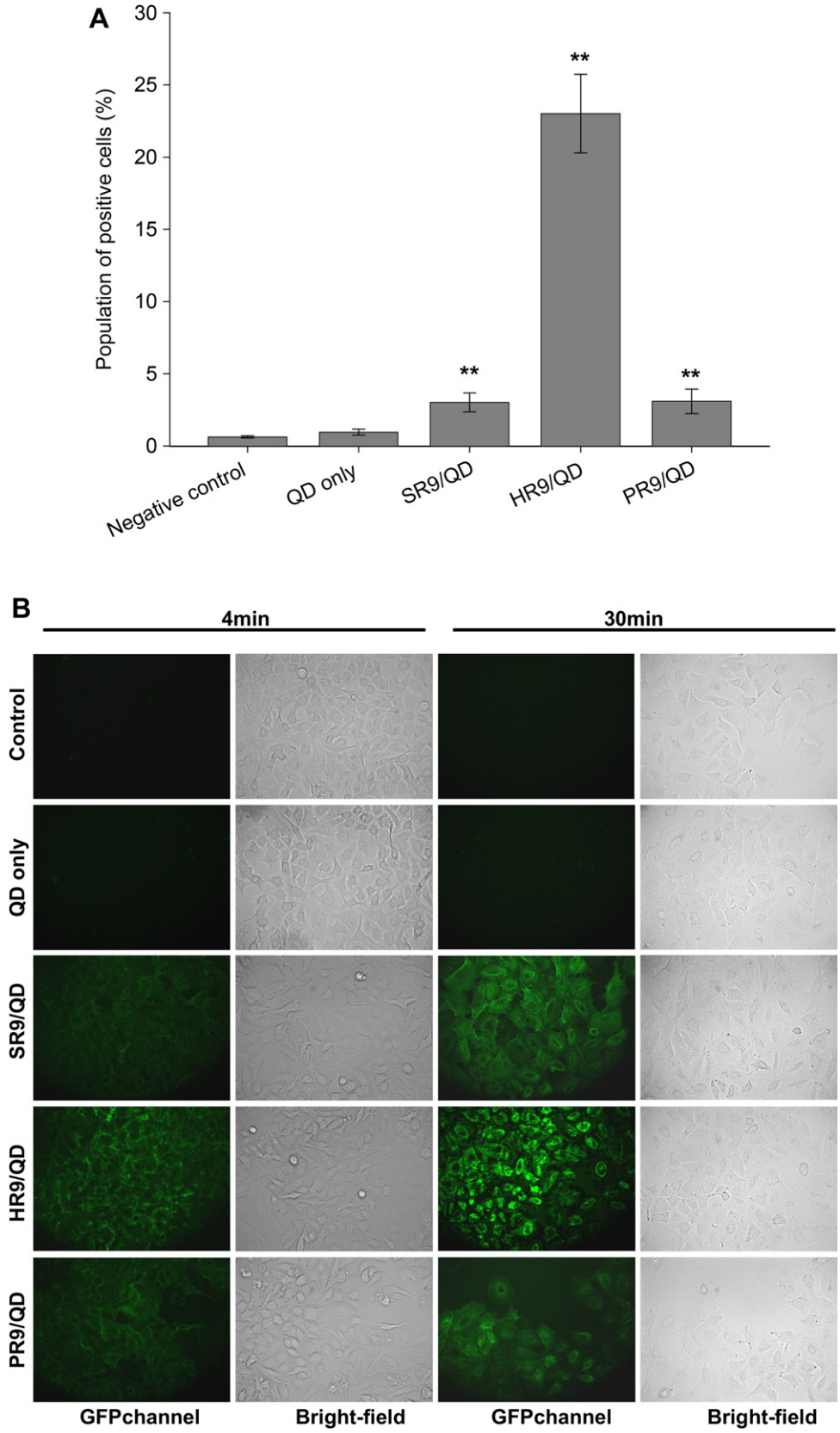

Fig. 4. Analysis of cellular internalization of CPP/QD complexes by direct membrane translocation. A: Histogram of the intracellularly fluorescent intensity from flow cytometry analysis. Cells were treated with PBS, QDs only or CPPs/QDs for 4 min. The *y*-axis shows the population of fluorescently positive cells. Significant differences were determined at $P < 0.05$ (*) and $P < 0.01$ (**). Data are presented as mean ± SD from 27 independent experiments in each treatment group. B: Fluorescent microscopy of cells treated with CPP/QDs for 4 and 30 min. The same treatments were performed in cells as described above, but analyzed using the BD pathway system. Cell morphologies are shown as bright-field images. All are shown at a magnification of 200×.

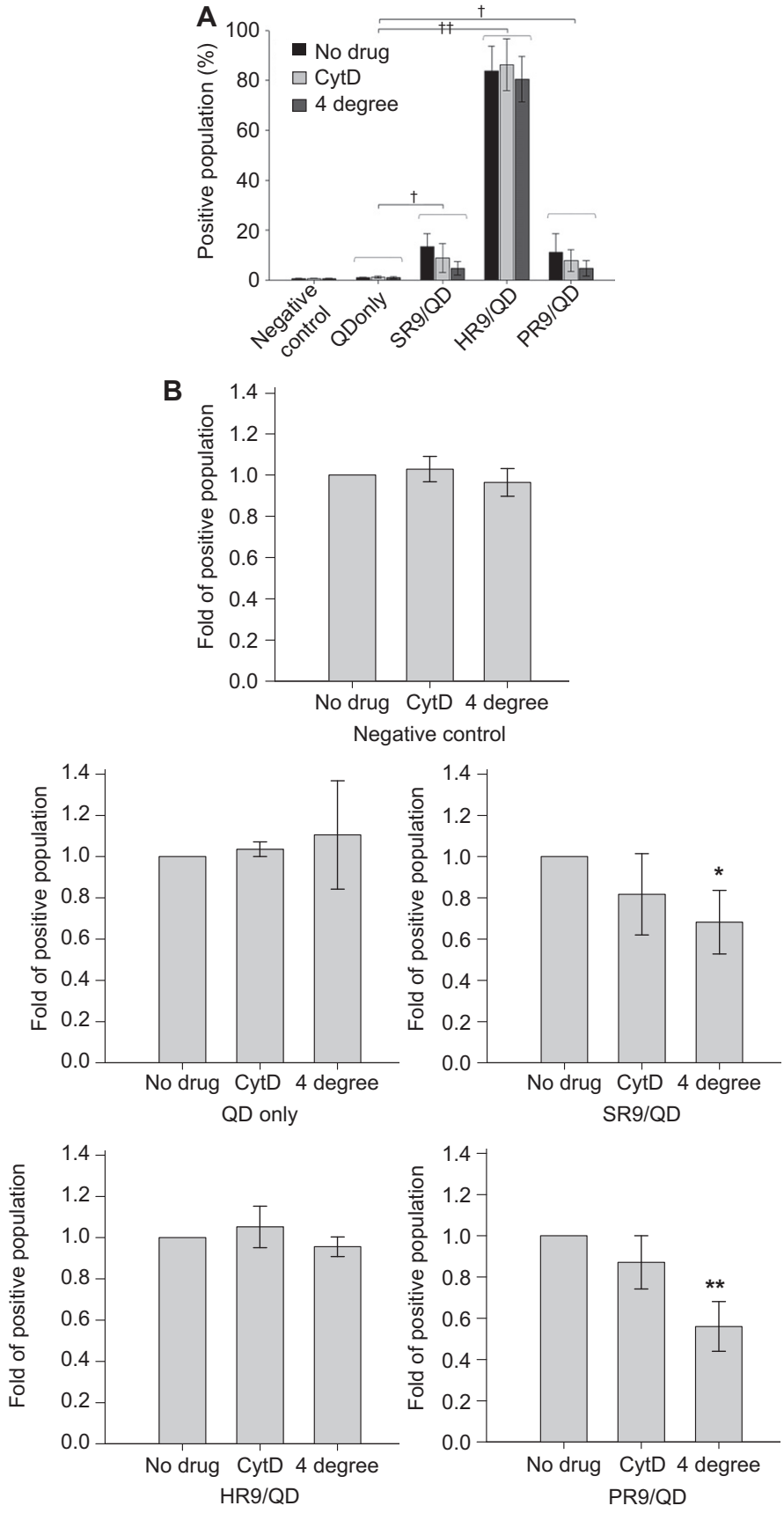

Fig. 5. Effects of endocytic inhibitors on membrane translocation of CPP/QD complexes. A: Transduction efficiency of CPPs/QDs. Cells treated with CPPs/QDs in the absence or presence of chemical (CytD) or physical (4 °C) endocytic inhibitors. Significant differences were determined at $P < 0.05$ (†) and $P < 0.01$ (††). Data are presented as mean ± SD from 5 independent experiments in each treatment group. B: Fractional change in transduction efficiency of CPPs/QDs. The negative control was cells without any treatments of CPPs or QDs, while the control was cells treated with QDs only. Significant differences were determined at $P < 0.05$ (*) and $P < 0.01$ (**). C: Fluorescent images of cells treated with QDs or CPP/QDs in the presence or absence of endocytic inhibitors. Cells were pretreated with or without CytD or 4 °C for 30 min, and then QDs or CPPs/QDs were added for 4 min. Images are shown from a BD pathway system at a magnification of 600×.

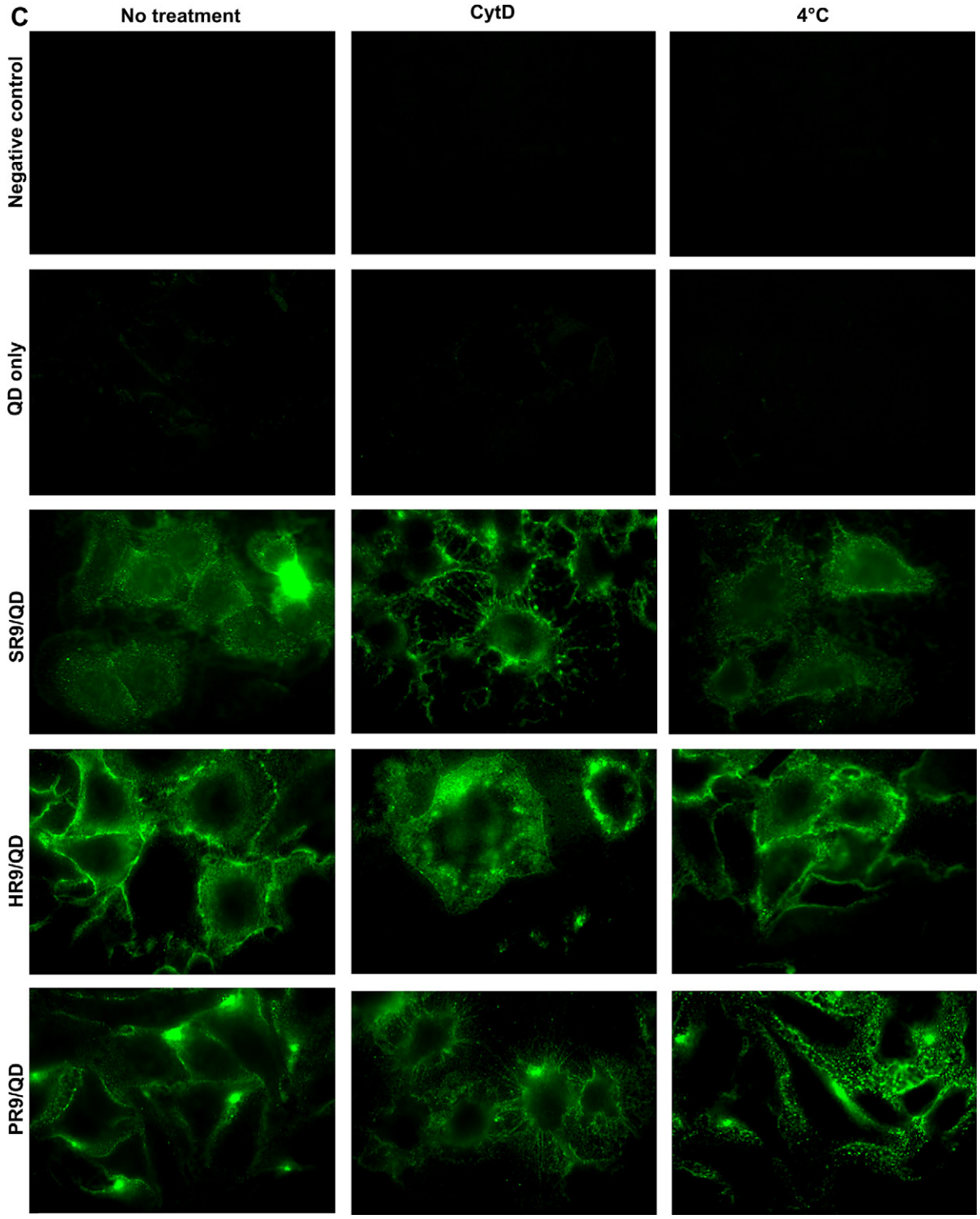

Fig. 5. (*continued*).

In a previous study, arginine-rich CPPs (SR9) were shown to facilitate protein transduction [15]. Thus, the delivery of SR9/QDs into human A549 cells for 1 h was used as a positive control, while we tested whether HR9 and PR9 were also capable of performing noncovalent transduction. The internal control (Fig. 2A, cells only) and the negative control which QDs were added without CPPs (Fig. 2B) were dark, but green fluorescence was observed in the positive control (Fig. 2C) using a confocal microscope. Green fluorescence was observed in cells treated with HR9/QDs (Fig. 2D) and PR9/QDs (Fig. 2E). HR9/QDs treated cells exhibited stronger fluorescence. These results indicated that both HR9/QDs and PR9/QDs had the abilities to pass through cell membranes.

To understand the kinetics of protein transduction, cells were treated with different kinds of CPP/QDs, and uptake was measured

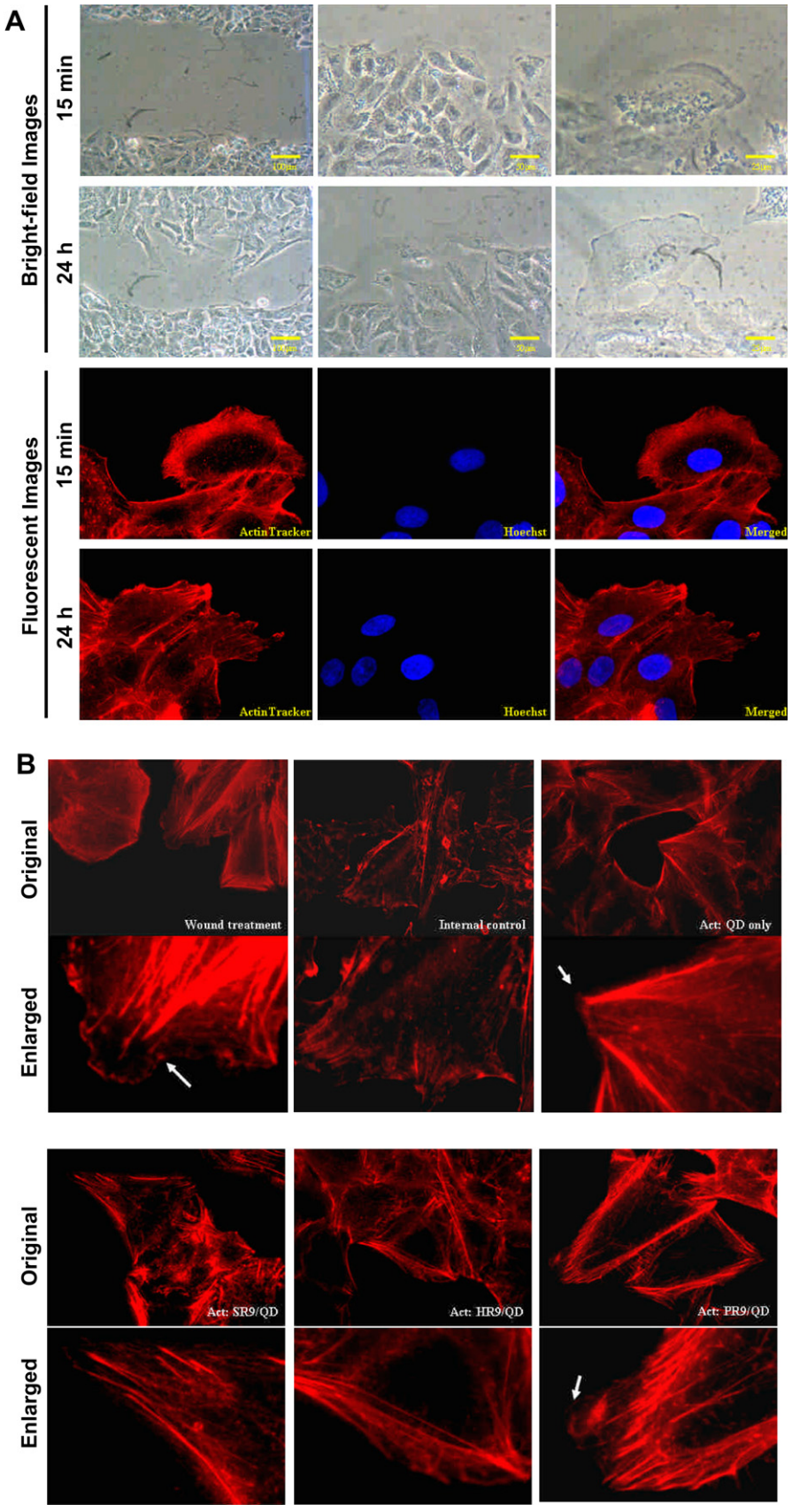

Fig. 6. Analysis of actin rearrangements during membrane translocation of CPP/QD complexes. A: Detection of actin rearrangements by the wound assay. Cells were wounded to induce the healing and migrations by actin rearrangements. Cell morphologies were observed at magnifications of 100× (upper-left and lower-left), 200× (upper-middle and lower-middle) and 400× (upper-right and lower-right) under the bright-field illumination at different time after injury (15 min and 24 h). Actins and nuclei were detected by Texas Red-X phalloidin in red fluorescence (upper-left and lower-left) and Hoechst 33342 in blue fluorescence (upper-middle and lower-middle), respectively. The merged images combined both red and blue fluorescence (upper-right and lower-right) at a magnification of 600×. B: Actin rearrangements in cells treated with CPP/QD complexes. The wound treatment caused membrane protruding and leading edges in cells in the positive group (up-left). Cells without any treatments of wound or QDs served as the internal control (up-middle). Experimental groups included cells treated with QDs only (upper-right), SR9/QDs (lower-left), HR9/QDs (lower-middle) and PR9/QDs (lower-right) for 4 min at 37 °C, respectively. White arrows indicate rough and protruding membrane edges. All groups were stained with Texas Red-X phalloidin and observed in RFP channel under original and enlarged magnifications.

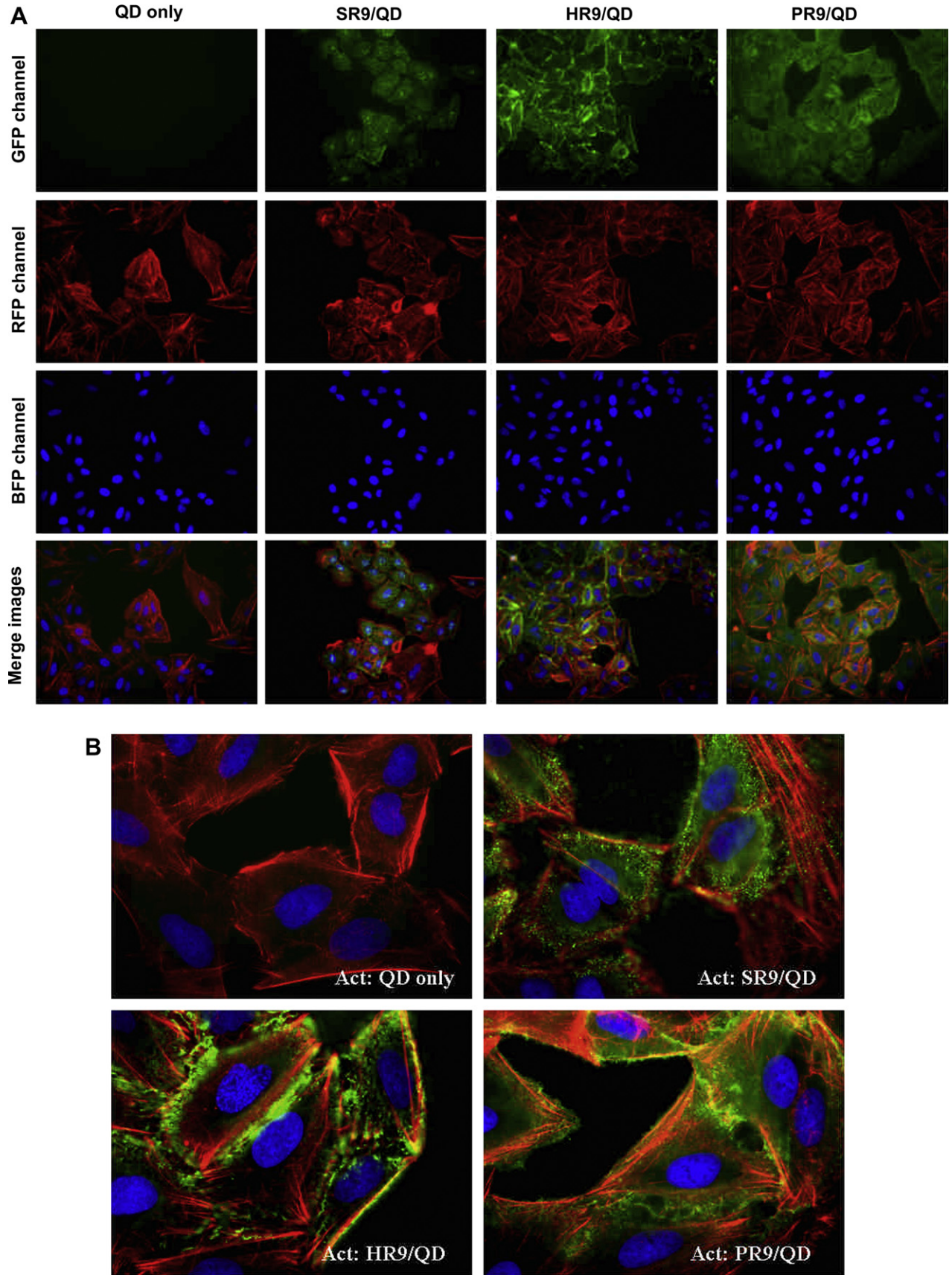

Fig. 7. Subcellular colocalization of CPP-delivered QDs. (A) Colocalization of QDs with F-actins and nuclei. Cells were treated with CPP/QDs for 4 min and stained with Texas Red-X phalloidin and Hoechst 33342. GFP, RFP and BFP channels to reveal the distribution of QDs, F-actins and nuclei, respectively. Overlaps between QDs and organelle trackers exhibit yellow color in merged GFP and RFP images, while overlaps between QDs and nuclei show cyan color in merged GFP and BFP images. Images were taken using a BD pathway system at a magnification of 200×. B: Enlarged colocalization images of QDs with F-actins and nuclei. Images from the above are shown at a magnification of 600×. C: Colocalization of QDs with microtubules and nuclei. Cells were stained with Cellular Lights MAP4-RFP, treated with CPP/QDs, and then stained with Hoechst 33342. D: Enlarged colocalization images of QDs with microtubules and nuclei (600×). E: Confocal colocalization images of QDs with microtubules and nuclei (600×). F: Colocalization of QDs with lysosomes and nuclei. Cells were treated with CPP/QDs and stained with LysoTracker DND-99 and Hoechst 33342. G: Enlarged colocalization images of QDs with lysosomes and nuclei (600×). H: Enlarged colocalization images of QDs with mitochondria and nuclei (600×). I: Enlarged colocalization images of QDs with lysosomes and nuclei after delivery by PR9 (600×). J: Enlarged colocalization images of QDs with F-actins and nuclei after delivery by PR9 (600×). K: Enlarged colocalization images of QDs with endoplasmic reticulum and nuclei after delivery by PR9 (600×).

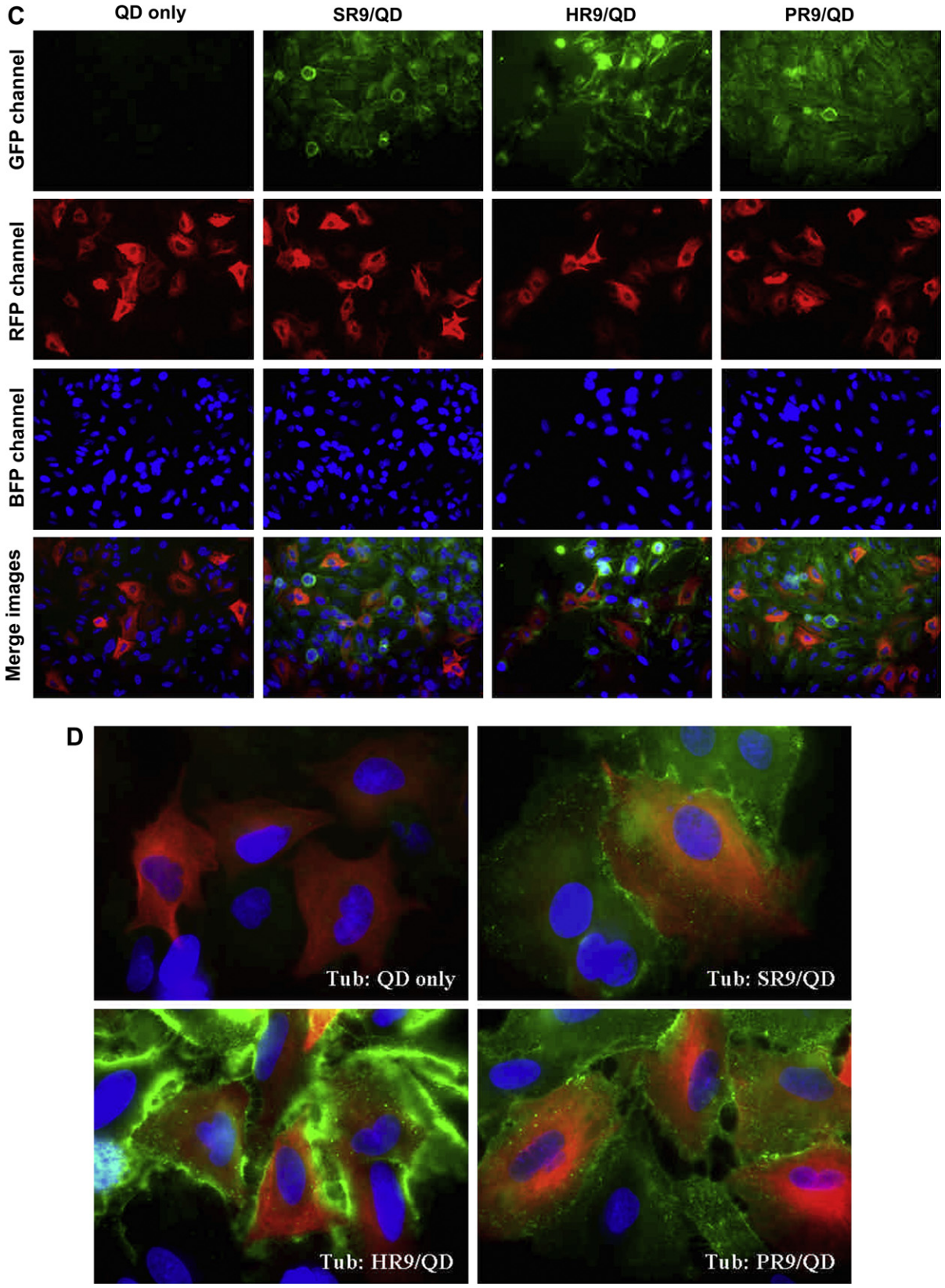

Fig. 7. (*continued*).

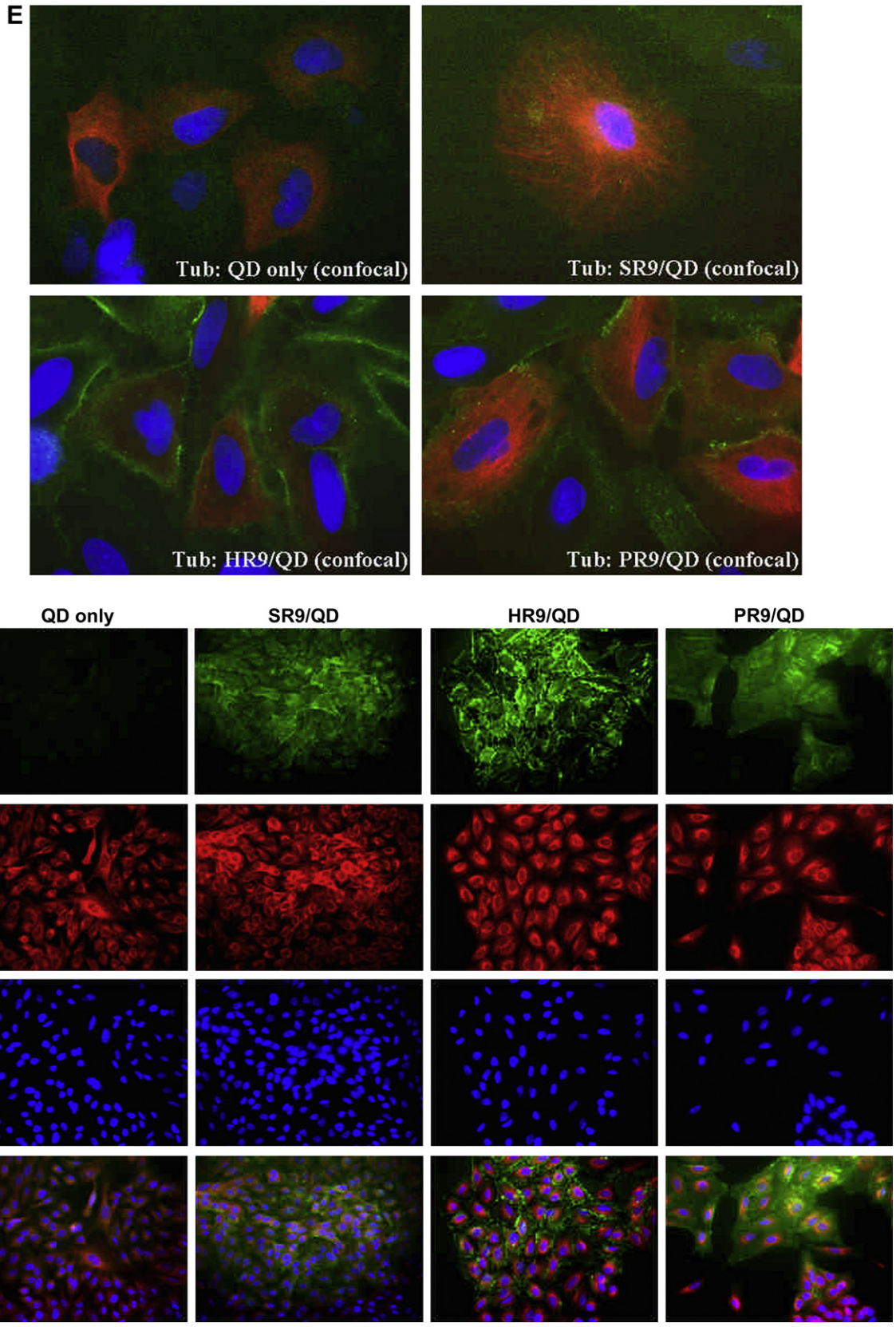

Fig. 7. (*continued*).

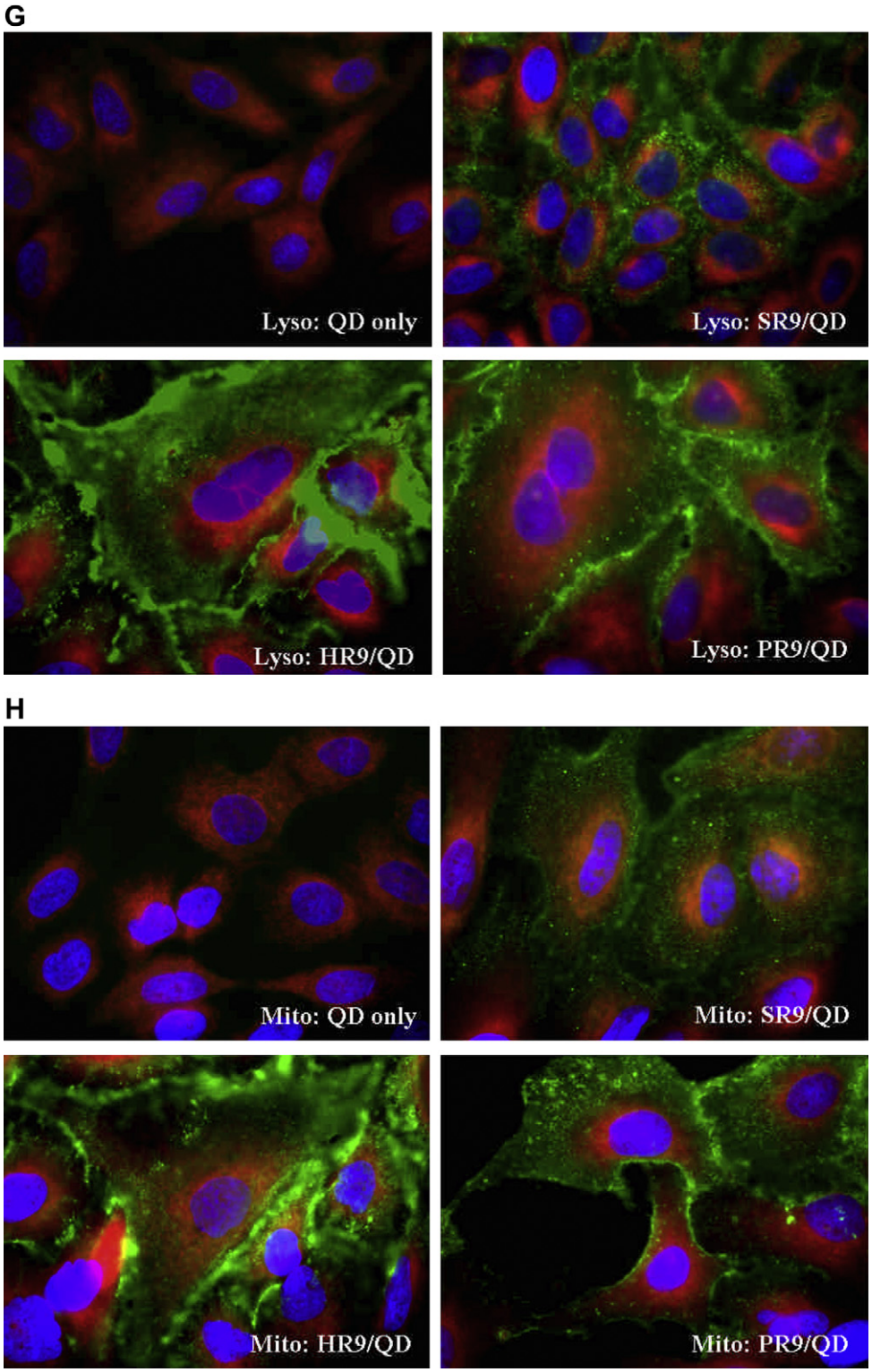

Fig. 7. (*continued*).

at various time points. At 0 min, green fluorescence was not detected in any group (Fig. 3). At 4 min, HR9-mediated transduction showed significantly higher uptake of QD than those of SR9 and PR9. The fraction of cells with fluorescence continued to increase over time. At 30 min, the HR9 group was 5.9 and 38.5 times higher than SR9 and PR9 uptake, respectively.

It takes approximately 5–15 min for endosome formation when materials are internalized via endocytic pathways [7,44]. Accordingly, a penetrating detection of cellular membrane at 4 min was used to visualize direct membrane translocation [39]. To study the membrane translocation, cells were incubated with different CPP/QDs for 4 min, and cell population fractions with

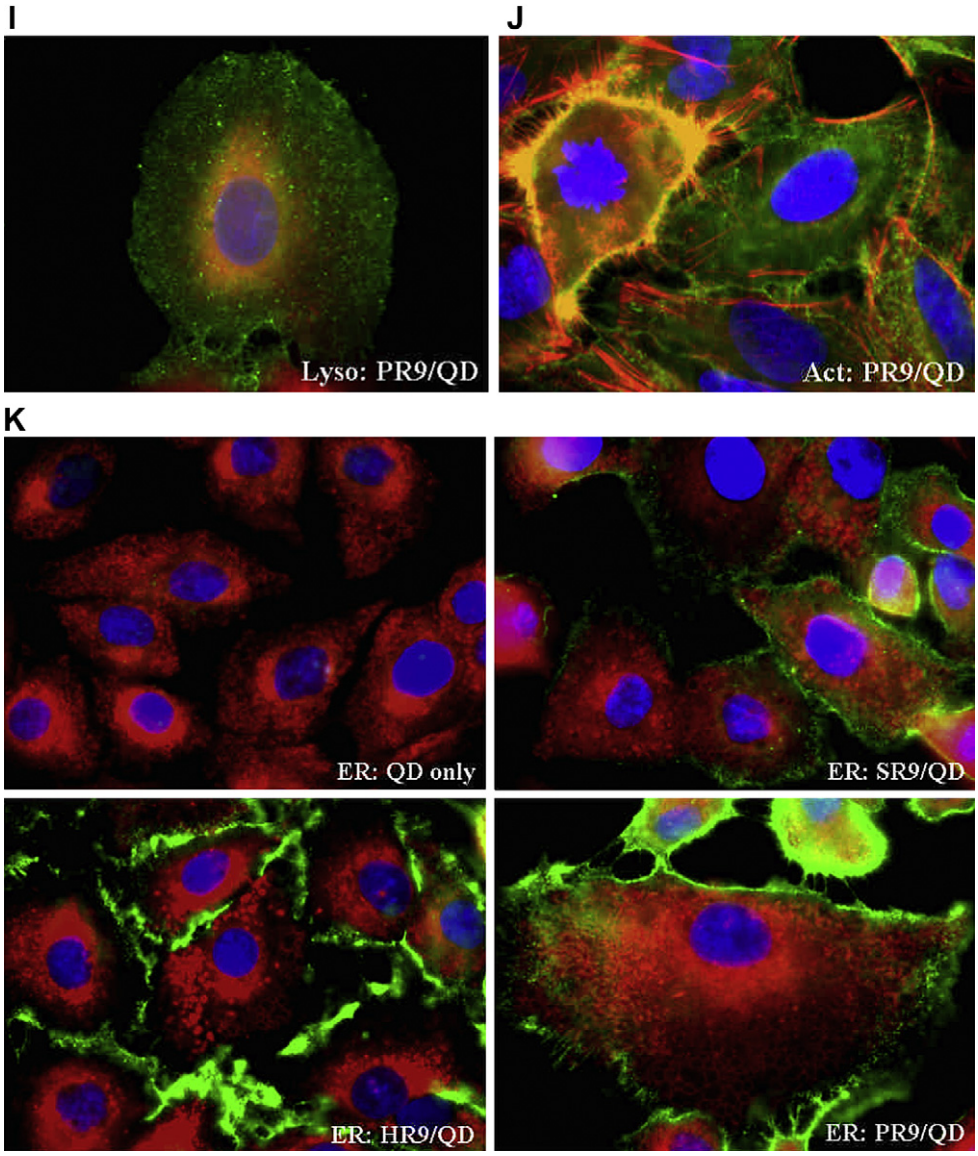

Fig. 7. (*continued*).

green fluorescence were analyzed by flow cytometry. Significant enhancement in transduction was detected in cells treated with SR9/QDs, HR9/QDs or PR9/QDs (Fig. 4A). Among them, cells incubated with HR9/QDs displayed the highest fraction of positive cells at 23.1 ± 2.7%, while cells treated with PBS, QDs, SR9/QDs and PR9/QDs showed population fractions of positive cells at 0.7 ± 0.1%, 1.0 ± 0.2%, 3.0 ± 0.7% and 3.1 ± 0.8%, respectively (Fig. 4A). Green fluorescence could be detected in groups with CPP/QDs in an extremely short period of 4 min, and stronger fluorescence was displayed in 30 min treatments (Fig. 4B). Accordingly, we believed that HR9/QDs entered cells via a direct membrane translocation because of their unusually high speed of penetration into cells [37].

CytD that interrupts F-actin polymerizations and low temperature that arrests all active transport are commonly used as a chemical and physical inhibitor of endocytosis, respectively [10–15,46]. Cells were treated QDs alone or CPP/QDs in the absence or presence of the inhibitor/condition (CytD or 4 °C). Groups treated with both CPP/QDs and CytD were compared to the group treated with both QDs only and CytD, while groups treated with CPP/QDs at 4 °C were compared to the group treated with QDs only at 4 °C (Fig. 5A). Conspicuously elevated transduction efficiencies were observed in cells treated with CPP/QDs in the absence of CytD or with low temperature. Moreover, the 4 min time course of this experiment suggested that cellular internalization of CPPs involves the direct membrane translocation (Fig. 5A). The increase in transduction efficiencies relative to respective control groups is shown in Fig. 5B. Treatments of CytD and 4 °C reduced transduction efficiencies of SR9/QDs and PR9/QDs (Fig. 5B). However, neither of these endocytic inhibitors reduced the transduction efficiency of HR9/QDs (Fig. 5B). Image data reconfirmed similar intensity of fluorescence in the absence or presence of endocytic inhibition with HR9/QDs (Fig. 5C). In contrast, the fluorescent intensity of cells treated with SR9/QDs was reduced in the presence of CytD and 4 °C (Fig. 5C). The fluorescent intensity of cells treated with PR9/QDs was decreased in the presence of CytD, although 4 °C treatment had no effect on fluorescent intensity (Fig. 5C). These results provide additional evidence that HR9 mediates direct membrane translocation for the intracellular delivery of non-covalently-complexed QDs.

A role of actin in eukaryotic endocytosis had been demonstrated [47]. The wound-healing process is a powerful stimulus for F-actin reorganization and cell migration [48]. We have performed a wound assay in order to understand actin rearrangement in the presence or absence of CPP/QDs. To perform this assay, we scraped the monolayer of A549 cells to form wounding lines and then stained cells with Texas Red-X phalloidin to visualize actin rearrangement. Membrane ruffling was observed at 15 min after cell injury (Fig. 6A). Cells stretched to heal wounds, and migrations were seen after 24 h (Fig. 6A, bright-field images). During injury, actins accumulate around the edges of membranes near wounds. Stress fibers then appear followed by actin rearrangements leading to rough and protruding membranes in 24 h (Fig. 6A, fluorescent images and Fig. 6B, up-left). Once the assay was established, cells were treated with QDs only or CPP/QDs followed by staining with Texas Red-X phalloidin. We found no difference in actin distributions between the internal control and the treatment with either SR9/QDs or HR9/QDs (Fig. 6B). Slightly protruding actins were observed in the group treated with QDs only, and stretched actin filaments around edges of cells with rough membranes were characteristic in the wound-treated group of PR9/QDs (Fig. 6B). These results suggest that the cellular entry of CPP/QDs is not mediated by actin-dependent endocytosis.

To reveal subcellular localization of CPP-delivered QDs, cells were treated with QDs only or with CPP/QDs, and stained with organelle-specific fluorescent markers, including Hoechst 33342, Texas Red-X phalloidin, Cellular Lights MAP4-RFP, LysoTracker DND-99, MitoTracker Deep Red FM and ER-Tracker Red for the visualization of nuclei, F-actins, microtubules, lysosomes, mitochondria and endoplasmic reticulums, respectively. The merged images showed that QDs were not associated with nuclei (Fig. 7), F-actins (Fig. 7A and B), microtubules (Fig. 7C–E), lysosomes (Fig. 7F and G) or mitochondria (Fig. 7H) of most cells after transduction delivery. However, we found orangey filaments in a few cells treated with PR9/QDs, indicating possible association of QDs with lysosomes (Fig. 7I), F-actins (Fig. 7J) and endoplasmic reticulums (Fig. 7K) after PR9-delivery. These results suggested that HR9/QDs internalization does not involve endocytosis.

Several chemical enhancers of membrane transduction [39,41] were used to evaluate the proposed membrane translocation of HR9/QDs. Cells were treated with either QDs only or CPP/QDs in the presence or absence of chemical enhancers and analyzed by flow cytometry (Fig. 8A–D). In groups of QDs only (Fig. 8A), SR9/QDs (Fig. 8B) and PR9/QDs (Fig. 8D), nearly identical distribution curves were exhibited. In contrast, divergent distribution curves were observed with cells treated with HR9/QDs (Fig. 8C). Both DMSO and ethanol have been reported to enhance transduction by disrupting the integrity of cell membranes [41]. Our quantitative data demonstrate that transduction efficiencies increase in the presence of DMSO or ethanol in CPP/QDs treated cells (Fig. 8E). As a membrane translocation enhancer, OA increases the hydrophobicity and generating crevices on cell membranes [49]. A significant increase in cell populations with fluorescence in treatments of either QDs only or CPPs/QDs supported the notion that OA is a potent enhancer for the direct membrane translocation (Fig. 8F). PB, a counter-anion of positively charged CPPs, also increases hydrophobicity and accelerates translocations across membranes [39]. We found that R9-GFP, a covalent CPP fusion protein [34,35], exhibited increased transduction in treatments with both R9-GFP and PB (Fig. 8G). Surprisingly, PB did not enhance the direct membrane translocation in either QDs only or CPP/QDs treated cells (Fig. 8G). This result may reflect the fact that negatively charged QDs are already the counter-anions of CPPs, and therefore PB cannot further increase the net hydrophobicities on membranes. These results suggest that DMSO, ethanol and OA enhance HR9/QD transduction by promoting the direct membrane translocation.

In a previous study, we found that QDs, SR9 and SR9/QDs do not cause any cytotoxicity in A549 cells up to 500 nM of QDs and 30 μM of SR9, the highest concentrations tested [15]. In this study, cells were treated with either CPPs or CPP/QDs (60:1) for 24 h. Viability assay showed that neither CPPs nor CPP/QDs cause cytotoxicity (Fig. 9).

4. Discussion

We used CPPs and carboxyl-functionalized QDs to form stably noncovalent CPP/QD complexes and characterized the rate, efficiency, potential mechanisms of cellular internalization, subcellular localization and cytotoxicity. One significant advantage of QDs in biomedical applications is that they can be used to study biological phenomena at the levels of none to slight cytotoxicity. For instance, adipose tissue-derived stem cells still maintained stem cell potency after transduction with QDs and octa-arginine (R8) [50]. Upon surface modifications, solubility of QDs can be improved making them suitable for biological applications. Further, conjugation with CPPs facilitates cellular uptake of QDs [21,27,51,52]. Though CPP-conjugated QDs raise the efficiency of cellular internalization, intracellular distributions of CPP-conjugated QDs have not yet been closely examined. Because uptake pathways determine intracellular destinations of QDs, characterization of the mechanism of cellular internalization is essential.

In this study, we investigated the transduction kinetics and the uptake mechanism of CPP/QDs (Fig. 3). Takeuchi et al. demonstrated that R8 incorporated with counter-anion PB increases hydrophobicity, leading to enhanced transduction within a few minutes at both 4 °C and 37 °C [39]. Prominent cytosolic diffusion of the carrier–cargo complex, instead of endosomal colocalization, was observed within 1–3 min. Further, there was no lactate dehydrogenase (LDH) release that indicated cell membrane integrity was not perturbed. Goda et al. observed energy-independent internalization of phospholipid polymers in HepG2 cells in 5 min [53]. Moreover, the internalization did not cause membrane bilayer disruption (i.e., no LDH release). Both studies pointed to direct endocytosis-independent membrane translocation within 5 min. Our translocation kinetics study with HR9/QDs displayed excellent penetration efficiency in less than 5 min (Fig. 4A). Therefore, the observed internalization of QDs by HR9 may involve direct membrane translocation. Our proposed mechanism is further supported by several complementary assays, such as pathway-specific inhibitors, actin rearrangement inhibitor, organelle-specific markers and membrane transduction enhancers.

Actin dynamics plays a critical role in the clathrin-, caveolae-mediated endocytosis, macropinocytosis and autophagy. Actin-rich membrane ruffles indicate an ongoing endocytic progress [47,54]. CytD, an F-actin polymerization inhibitor, blocks actin rearrangements, leading to suppression of clathrin-, caveolae-mediated endocytosis, macropinocytosis and micropinocytosis formations [31,32,55–57]. Our inhibitor studies and colocalization data re-affirm that entry of HR9/QDs into cells is not associated with endocytosis based upon the facts that: 1) both CytD and 4 °C (inhibition of energy-dependent endocytosis by depletion of ATP [58]) could not reduced the internalization of HR9/QDs (Fig. 5), 2) no colocalization was found between HR9/QDs and organelles, such as actins and microtubules (Fig. 6 and Fig. 7A–E and 3) HR9/QDs were not trapped in lysosomes (Fig. 7F and G).

Lo and Wang designed a C-5H-TAT-5H-C peptide, consisting of a PTD of TAT flanked by 5-histidine residues and a cysteine at both ends [42]. This peptide promoted internalization of a nonviral DNA vector and increased its gene expression. They proposed that the

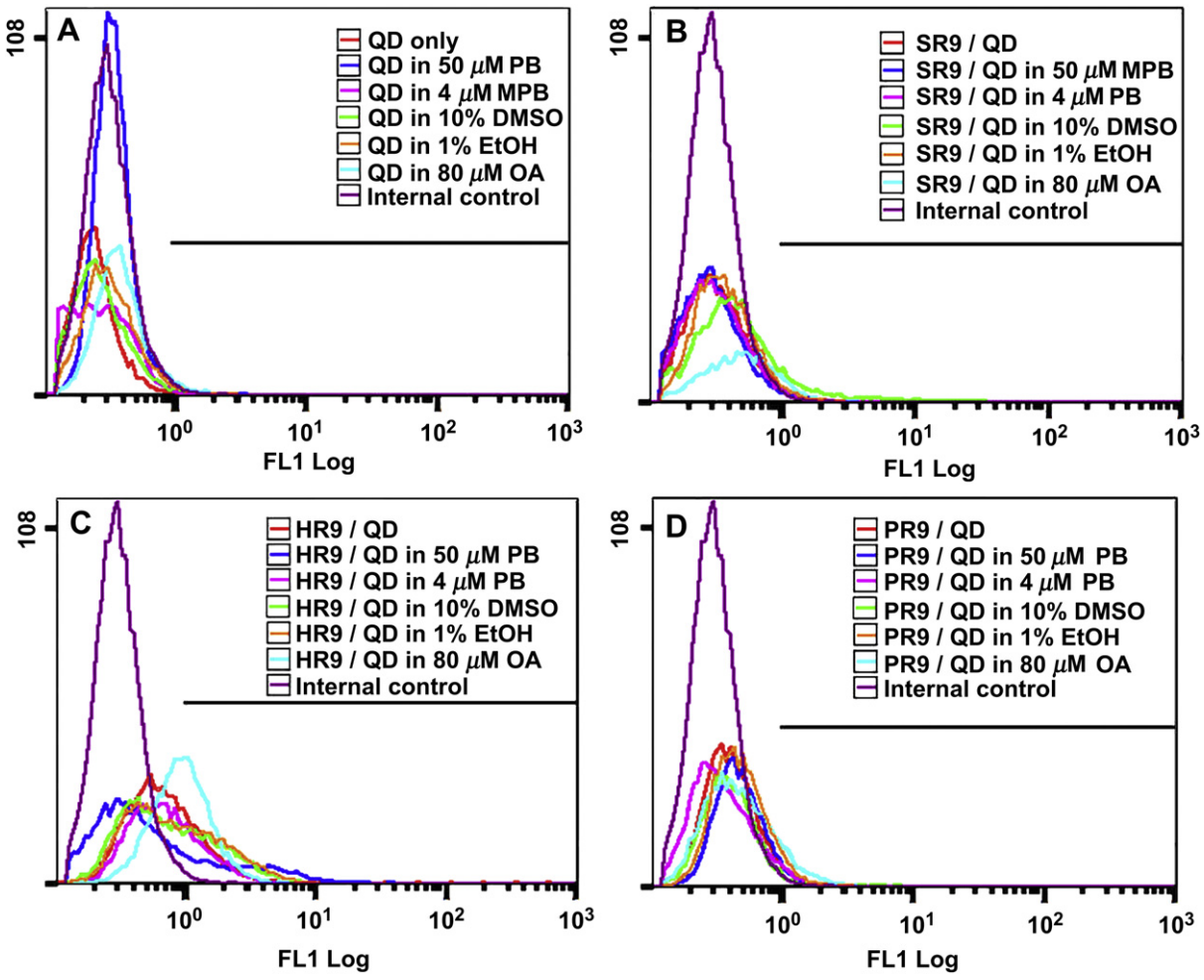

Fig. 8. Effects of transduction enhancers on membrane translocation of CPP/QD complexes. A–D: Translocation efficiency of CPP/QD complexes in the presence or absence of transduction enhancers. Cells treated with different transduction enhancers, and then protein transduction experiments were performed for 4 min at 37 °C. Fluorescent cells were detected by flow cytometry. Fluorescent positive cells are recognized by cell counts (*y*-axis) at the fluorescent gate region (*x*-axis) with FL1 > 1. E: Translocation enhancement by perforating agents. Cells were pretreated with 10% DMSO or 1% ethanol for 1 h, and then protein transduction experiments were conducted. The population of fluorescent positive cells is shown on the *y*-axis. Significant differences were determined at $P < 0.05$ (* or †) and $P < 0.01$ (** or ††). Data are presented as mean ± SD from 5 independent experiments in each treatment group. F: Translocation enhancement by OA, a transdermal enhancer. Cells were treated with 80 μM of OA, CPP/QDs for 4 min and analyzed by flow cytometry. Cells treated with the OA solvent (ethanol) served as a mock treatment. Significant differences were determined at $P < 0.05$ (* or †) and $P < 0.01$ (** or ††). Data are presented as mean ± SD from 3 independent experiments in each treatment group. G: Translocation enhancement by PB, a hydrophobic counter-ion. Cells were incubated with either 4 μM or 50 μM of PB for 2 min, and then protein transduction experiments were carried out for 4 min. Cells treated with 30 μM of R9-GFP in the presence or absence of PB served as positive controls. Significant differences were determined at $P < 0.05$ (* or †) and $P < 0.01$ (** or ††). Data are presented as mean ± SD from 7 independent experiments in each treatment group.

imidazole groups of histidine facilitated proton influx (proton sponge effect) to endosomes, leading to endosomal bursting [42]. Similarly, the transduction efficiency of polylysine partially substituted with histidyl residues was substantially increased via proton sponge effect [59]. Although both studies demonstrated proton sponge effects of the imidazole groups of histidine, another study showed that nona-histidine (H9), as well as nona-lysine (K9), was incapable of protein transduction [60]. Thus, it should be noted that membrane transduction involves multiple factors, such as degree of hydrophobicity, peptide structural transitions and membrane composition [61].

Rose and Wolfenden suggested that cysteine was the most hydrophobic amino acid, and histidine belonged to moderately hydrophobic residues [62]. By the same token, both Pas-modification and N-terminal acylation of arginine-rich CPPs (PasR8 and C6R8) were developed to significantly improve delivery efficiency by raising hydrophobicity [43,46]. Studies have shown that the guanidinium-head groups of arginines were crucial for cellular uptake due to their interactions with membrane phospholipids, as substituting nitrogen of guanidine with oxygen reduced the ability of transduction [60,63]. It supports this notion that the penetration rate of the guanidinium-rich peptides was about three times faster than that of the PTD of TAT [64]. The head groups of arginine-rich peptides inserted into lipid bilayers produced local membrane distortion leading to transient pore formation on membranes [37,65]. Armstrong and Baldwin indicated that the histidine residues at positions near C-termini can stabilize the secondary structure of any peptides [66]. This information motivated us to design the HR9 peptide (C-5H-R9-5H-C), a nona-arginine flanked by a cysteine and 5 histidines at both ends. We hypothesized that histidine and cysteine residues in HR9 increase the net hydrophobicity and facilitate HR9/QDs passing through lipid bilayers by the direct membrane translocation. The hypothesis was supported by our observations: while SR9 and PR9 possessed similar transduction ability, HR9 penetrated much faster than SR9 and PR9 did (Figs. 3 and 4). According to the existing references [43,46,60,62–66] and our

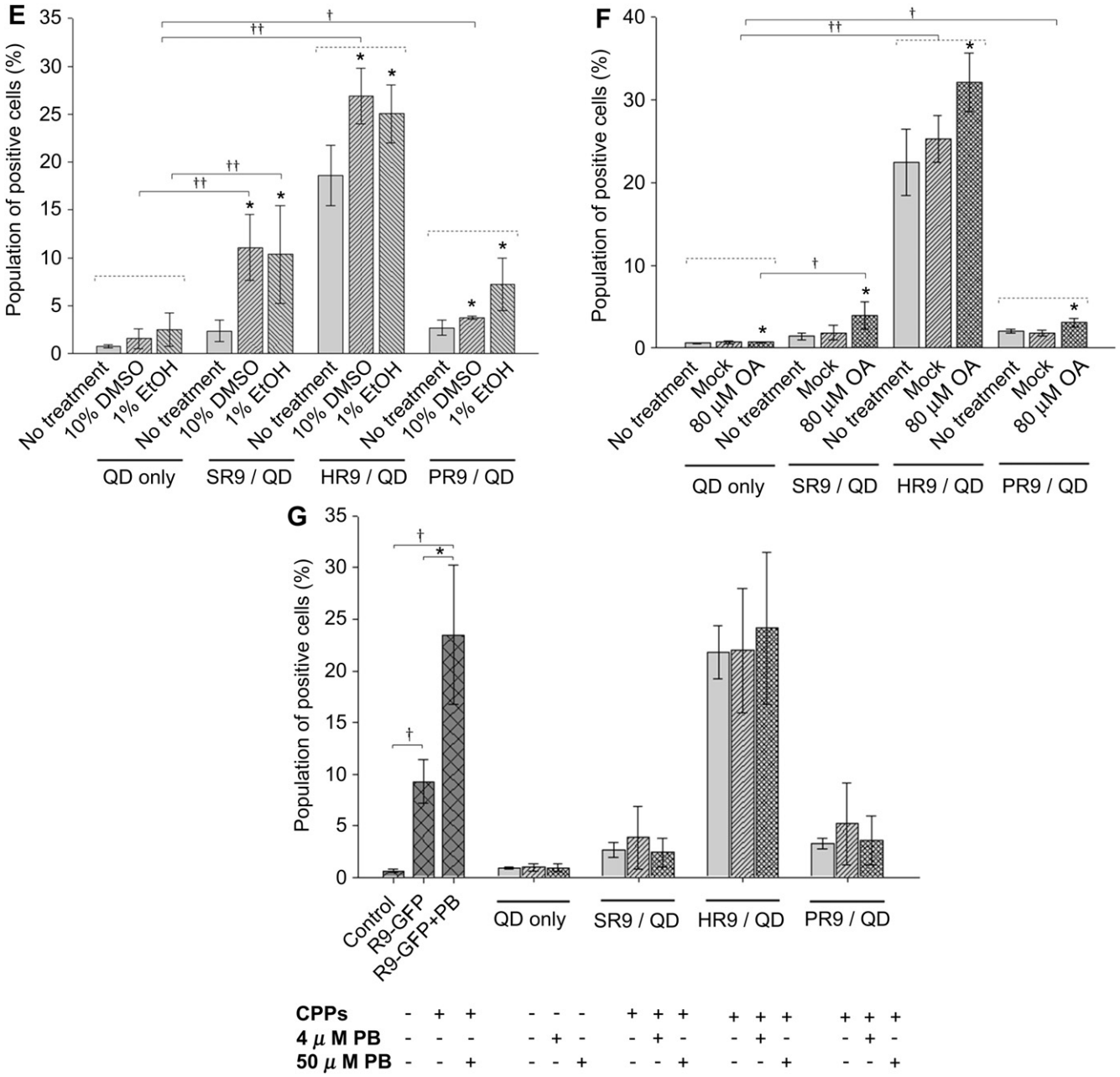

Fig. 8. (*continued*).

observations in this study, the differential kinetics of these three peptides might be a function of hydrophobicity and peptide structural transitions. Guanidinium-head groups of arginines may initiate HR9's contact with cell membrane. Hydrophobic cysteines and histidines further facilitate the peptide's interactions with membrane phospholipids and stabilize the secondary structure of peptides. The interactions induce local distortions to the phospholipid bilayer in comparison with its resting structure and reduce the free-energy barrier as an arginine side chain translocates attracted by phosphate groups on the distal side. This process helps the nucleation and the formation of a toroidal pore. Once the pore is formed, the peptides translocate by diffusing on the surface of the pore. Additional studies on molecular dynamics modeling and three dimensional peptide–phospholipid interactions are desirable to attest the proposed dynamic interactions of our particular peptide.

Most transduction enhancers promote traverse by increasing either hydrophobicity or pore formations on cell membranes. For instance, DMSO and OA increase both hydrophobicity and pore formations [41,49], while ethanol facilitates pore formations [67]. These three agents have been used to enhance transdermal delivery of pharmaceuticals [68–70]. Therefore, we utilized them to further understand their influence on uptake and direct membrane transduction of CPP/QDs. Our experiments revealed that they have differential effects on CPP-mediated transduction of QDs (Fig. 8E and F). According to previous studies, the low concentrations of DMSO, ethanol and OA we used in this study should not perforate cell membrane but only increase fluidity of the membrane's hydrophobic core [41,45]. PB possesses an aromatic hydrophobic moiety and contains negatively charged carboxyl groups, thus a counter-anion to CPPs. A previous study suggested that the enhanced transduction of CPPs is the

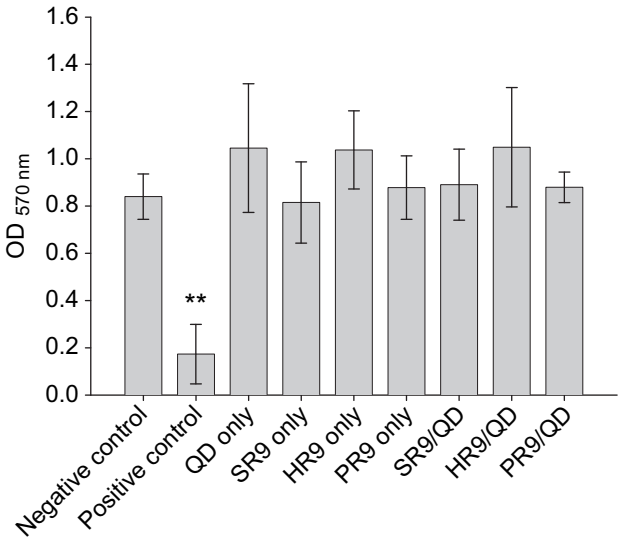

Fig. 9. Cytotoxicity of CPP/QD complexes. Cells were incubated at 37 °C for 24 h with 100 nM of QDs only, 6 μM of CPPs only or CPP/QDs. Cells mock-treated and treated with DMSO for 24 h served as negative and positive controls, respectively. The SRB assay was used to evaluate cytotoxicity. Significant differences were determined at $P < 0.01$ (**). Data are presented as mean ± SD from 3 independent experiments in each treatment group.

consequence of the increased electrostatic interactions between CPPs and PB followed by the increased net cell membrane hydrophobicity due to PB's aromatic hydrophobic moiety [39]. On the other hand, another pointed out that PB leads to cellular binding, not intracellular delivery, of polyarginine-QDs [71]. In our study, PB increases R9-GFP entry (Fig. 8G). This observation supported the notion that PB could interact with R9-GFP as a counter-anion and facilitate binding of R9-GFP to cell membrane. However, we did not observe significantly enhanced delivery of either QDs or CPP/QDs in the presence of PB (Fig. 8G). We proposed this is a consequence of PB and QDs becoming competitors to interact with CPPs.

5. Conclusions

We have demonstrated that modified CPPs (HR9 and PR9) can interact with carboxylated QDs, increasing transduction efficiency. These HR9/QDs did not enter cells via an endocytic pathway, since chemical and physical inhibitors could not reduce transduction efficiency. The mechanism of entrance into cells for HR9/QDs involved neither F-actin polymerization nor microtubule rearrangements, but rather by the direct membrane translocation; they would be trapped in neither endosomes nor lysosomes. Nontoxic CPP/QDs (such as SR9/QDs, HR9/QDs and PR9/QDs) have a number of superior features, and HR9 appears to be an excellent carrier for the delivery of medical cargoes.

Acknowledgements

We are grateful to Dr. Robert S. Aronstam for technical editing. This work was supported by Award Number R15EB009530 from the National Institutes of Health (to Y.-W. H.) and the National Science Council (NSC 97-2621-B-259-003-MY3) of Taiwan (to H.-J. L.).

Appendix

Figures with essential colour discrimination. Certain figures in this article, particularly Figures 1,2 and 4–8 are difficult to interpret in black and white. The full colour images can be found in the online version, at doi:10.1016/j.biomaterials.2011.01.041.

References

[1] Mukherjee S, Ghosh RN, Maxfield FR. Endocytosis Physiol Rev 1997;77(3):759–803.
[2] Luzio JP, Poupon V, Lindsay MR, Mullock BM, Piper RC, Pryor PR. Membrane dynamics and the biogenesis of lysosomes. Mol Membr Biol 2003;20(2):141–54.
[3] Jo J, Tabata Y. Non-viral gene transfection technologies for genetic engineering of stem cells. Eur J Pharm Biopharm 2008;68(1):90–104.
[4] Wiesman Z, Dom NB, Sharvit E, Grinberg S, Linder C, Heldman E, et al. Novel cationic vesicle platform derived from vernonia oil for efficient delivery of DNA through plant cuticle membranes. J Biotechnol 2007;130(1):85–94.
[5] Stewart KM, Horton KL, Kelley SO. Cell-penetrating peptides as delivery vehicles for biology and medicine. Org Biomol Chem 2008;6(13):2242–55.
[6] Wagstff KM, Jans DA. Protein transduction: cell penetrating peptides and their therapeutic applications. Curr Med Chem 2006;13(12):1371–87.
[7] Zorko M, Langel U. Cell-penetrating peptides: mechanism and kinetics of cargo delivery. Adv Drug Deliv Rev 2005;57(4):529–45.
[8] Eiríksdóttir E, Konate K, Langel U, Divita G, Deshayes S. Secondary structure of cell-penetrating peptides controls membrane interaction and insertion. Biochim Biophys Acta 2010;1798(6):1119–28.
[9] Eiríksdoćttir E, Mager I, Lehto T, El Andaloussi S, Langel U. Cellular internalization kinetics of (luciferin-)cell-penetrating peptide conjugates. Bioconjug Chem 2010;21(9):1662–72.
[10] Chang M, Chou JC, Chen CP, Liu BR, Lee HJ. Noncovalent protein transduction in plant cells by macropinocytosis. New Phytol 2007;174(1):46–56.
[11] Liu BR, Chou JC, Lee HJ. Cell membrane diversity in noncovalent protein transduction. J Membr Biol 2008;222(1):1–15.
[12] Chen CP, Chou JC, Liu BR, Chang M, Lee HJ. Transfection and expression of plasmid DNA in plant cells by an arginine-rich intracellular delivery peptide without protoplast preparation. FEBS Lett 2007;581(9):1891–7.
[13] Wang YH, Hou YW, Lee HJ. An intracellular delivery method for siRNA by an arginine-rich peptide. J Biochem Biophys Methods 2007;70(4):579–86.
[14] Liu K, Lee HJ, Leong SS, Liu CL, Chou JC. A bacterial indole-3-acetyl-L-aspartic acid hydrolase inhibits mung bean (*Vigna radiata* L.) seed germination through arginine-rich intracellular delivery. J Plant Growth Regul 2007;26(3):278–84.
[15] Liu BR, Li JF, Lu SW, Lee HJ, Huang YW, Shannon KB, et al. Cellular internalization of quantum dots noncovalently conjugated with arginine-rich cell-penetrating peptides. J Nanosci Nanotechol 2010;10(10):6534–43.
[16] Wadia JS, Dowdy SF. Protein transduction technology. Curr Opin Biotechnol 2002;13(1):52–6.
[17] Tunnemann G, Ter-Avetisyan G, Martin RM, Stockl M, Herrmann A, Cardoso MC. Live-cell analysis of cell penetration ability and toxicity of oligo-arginines. J Pept Sci 2008;14(4):469–76.
[18] Chen F, Gerion D. Fluorescent CdSe/ZnS nanocrystal-peptide conjugates for long-term, nontoxic imaging and nuclear targeting in living cells. Nano Lett 2004;4(10):1827–32.
[19] Michalet X, Pinaud FF, Bentolila LA, Tsay JM, Doose S, Li JJ, et al. Quantum dots for live cells, in vivo imaging, and diagnostics. Science 2005;307(5709):538–44.
[20] Delehanty JB, Mattoussi H, Medintz IL. Delivering quantum dots into cells: strategies, progress and remaining issues. Anal Bioanal Chem 2009;393(4):1091–105.
[21] Xue FL, Chen JY, Guo J, Wang CC, Yang WL, Wang PN, et al. Enhancement of intracellular delivery of CdTe quantum dots (QDs) to living cells by TAT conjugation. J Fluoresc 2007;17(2):149–54.
[22] Koshman YE, Waters SB, Walker LA, Los T, de Tombe P, Goldspink PH, et al. Delivery and visualization of proteins conjugated to quantum dots in cardiac myocytes. J Mol Cell Cardiol 2008;45(6):853–6.
[23] Wei Y, Jana NR, Tan SJ, Ying JY. Surface coating directed cellular delivery of TAT-functionalized quantum dots. Bioconjug Chem 2009;20(9):1752–8.
[24] Liu BR, Huang YW, Chiang HJ, Lee HJ. Cell-penetrating peptide-functionized quantum dots for intracellular delivery. J Nanosci Nanotechnol 2010;10(12):7897–905.
[25] Xu Y, Liu BR, Lee HJ, Shannon KS, Winiarz JG, Wang TC, et al. Nona-arginine facilitates delivery of quantum dots into cells via multiple pathways. J Biomed Biotechnol 2010;2010:948543.
[26] Bharali DJ, Lucey DW, Jayakumar H, Pudavar HE, Prasad PN. Folate-receptor-mediated delivery of InP quantum dots for bioimaging using confocal and two-photon microscopy. J Am Chem Soc 2005;127(32):11364–71.
[27] Ruan G, Agrawal A, Marcus AI, Nie S. Imaging and tracking of TAT peptide-conjugated quantum dots in living cells: new insights into nanoparticle uptake, intracellular transport, and vesicle shedding. J Am Chem Soc 2007;129(47):14759–66.
[28] Tünnemann G, Martin RM, Haupt S, Patsch C, Edenhofer F, Cardoso MC. Cargo-dependent mode of uptake and bioavailability of TAT-containing proteins and peptides in living cells. FASEB J 2006;20(11):1775–84.
[29] Jiao CY, Delaroche D, Burlina F, Alves ID, Chassaing G, Sagan S. Translocation and endocytosis for cell-penetrating peptides internalization. J Biol Chem 2009;284(49):33957–65.

[30] Kawamura KS, Sung M, Bolewska-Pedyczak E, Gariepy J. Probing the impact of valency on the routing of arginine-rich peptides into eukaryotic cells. Biochemistry 2006;45(4):1116–27.
[31] Fervari A, Pellegrini V, Arcangeli C, Fittipaldi A, Giacca M, Beltram F. Caveolae-mediated internalization of extracellular HIV-1 Tat fusion proteins visualized in real time. Mol Ther 2003;8(2):284–94.
[32] Fittipaldi A, Ferrari A, Zoppé M, Arcangeli C, Pellegrini V, Beltram F, et al. Cell membrane lipid rafts mediate caveolar endocytosis of HIV-1 TAT fusion proteins. J Biol Chem 2003;278(36):34141–9.
[33] Wadia JS, Stan RV, Dowdy SF. Transducible TAT-HA fusogenic peptide enhances escape of TAT-fusion proteins after lipid raft macropinocytosis. Nat Med 2004;10(3):310–5.
[34] Hu JW, Liu BR, Wu CY, Lu SW, Lee HJ. Protein transport in human cells mediated by covalently and noncovalently conjugated arginine-rich intracellular delivery peptides. Peptides 2009;30(9):1669–78.
[35] Lu SW, Hu JW, Liu BR, Lee CY, Li JF, Chou JC, et al. Arginine-rich intracellular delivery peptides synchronously deliver covalently and noncovalently linked proteins into plant cells. J Agric Food Chem 2010;58(4):2288–94.
[36] El-Sayed A, Futaki S, Harashima H. Delivery of macromolecules using arginine-rich cell-penetrating peptides: ways to overcome endosomal entrapment. AAPS J 2009;11(1):13–22.
[37] Herce HD, Garcia AE, Litt J, Kane RS, Martin P, Enrique N, et al. Arginine-rich peptides destabilize the plasma membrane, consistent with a pore formation translocation mechanism of cell-penetrating peptides. Biophys J 2009;97(7):1917–25.
[38] Li S, Su Y, Luo W, Hong M. Water-protein interactions of an arginine-rich membrane peptide in lipid bilayers investigated by solid-state nuclear magnetic resonance spectroscopy. J Phys Chem B 2010;114(11):4063–9.
[39] Takeuchi T, Kosuge M, Tadokoro A, Sugiura Y, Nishi M, Kawata M, et al. Direct and rapid cytosolic delivery using cell-penetrating peptides mediated by pyrenebutyrate. ACS Chem Biol 2006;1(5):299–303.
[40] Yang S, Coles DJ, Esposito A, Mitchell DJ, Toth I, Minchin RF. Cellular uptake of self-assembled cationic peptide-DNA complexes: multifunctional role of the enhancer chloroquine. J Control Release 2009;135(2):159–65.
[41] Gurtovenko AA, Anwar J. Modulating the structure and properties of cell membranes: the molecular mechanism of action of dimethyl sulfoxide. J Phys Chem B 2007;111(35):10453–60.
[42] Lo SL, Wang S. An endosomolytic TAT peptide produced by incorporation of histidine and cysteine residues as a nonviral vector for DNA transfection. Biomaterials 2008;29(15):2408–14.
[43] Takayama K, Nakase I, Michiue H, Takeuchi T, Tomizawa K, Matsui H, et al. Enhanced intracellular delivery using arginine-rich peptides by the addition of penetration accelerating sequences (Pas). J Control Release 2009;138(2):128–33.
[44] Jones NL, Willingham MC. Modified LDLs are internalized by macrophages in part via macropinocytosis. Anat Rec 1999;255(1):57–68.
[45] Mastrangelo AM, Jeitner TM, Eaton JW. Oleic acid increases cell surface expression and activity of CD11b on human neutrophils. J Immunol 1998;161(8):4268–75.
[46] Katayama S, Hirose H, Takayama K, Nakase I, Futaki S. Acylation of octaarginine: implication to the use of intracellular delivery vectors. J Control Release 2011;149(1):29–35.
[47] Smythe E, Ayscough KR. Actin regulation in endocytosis. J Cell Sci 2006;119(22):4589–98.
[48] Malliri A, Symons M, Hennigan RF, Hurlstone AF, Lamb RF, Wheeler T, et al. The transcription factor AP-1 is required for EGF-induced activation of rho-like GTPases, cytoskeletal rearrangements, motility, and in vitro invasion of A431 cells. J Cell Biol 1998;143(4):1087–99.
[49] Mak VH, Potts RO, Guv RH. Percutaneous penetration enhancement in vivo measured by attenuated total reflectance infrared spectroscopy. Pharm Res 1990;7(8):835–41.
[50] Yukawa H, Kagami Y, Watanabe M, Oishi K, Miyamoto Y, Okamoto Y, et al. Quantum dots labeling using octa-arginine peptides for imaging of adipose tissue-derived stem cells. Biomaterials 2010;31(14):4094–103.
[51] Lei Y, Tang H, Yao L, Yu R, Feng M, Zou B. Applications of mesenchymal stem cells labeled with TAT peptide conjugated quantum dots to cell tracking in mouse body. Bioconjug Chem 2008;19(2):421–7.
[52] Chen B, Liu Q, Zhang Y, Xu L, Fang X. Transmembrane delivery of the cell-penetrating peptide conjugated semiconductor quantum dots. Langmuir 2008;24(20):11866–71.
[53] Goda T, Goto Y, Ishihara K. Cell-penetrating macromolecules: direct penetration of amphipathic phospholipid polymers across plasma membrane of living cells. Biomaterials 2010;31(8):2380–7.
[54] Lázaro-Diéguez F, Knecht E, Egea G. Clearance of a Hirano body-like F-actin aggresome generated by jasplakinolide. Autophagy 2008;4(5):717–20.
[55] Holzer AK, Howell SB. The internalization and degradation of human copper transporter 1 following cisplatin exposure. Cancer Res 2006;66(22):10944–52.
[56] Shurety W, Bright NA, Luzio JP. The effects of cytochalasin D and phorbol myristate acetate on the apical endocytosis of ricin in polarised Caco-2 cells. J Cell Sci 1996;109(12):2927–35.
[57] Nakase I, Niwa M, Takeuchi T, Sonomura K, Kawabata N, Koike Y, et al. Cellular uptake of arginine-rich peptides: roles for macropinocytosis and actin rearrangement. Mol Ther 2004;10(6):1011–22.
[58] Sudhakaran PR, Prinz R, Figura KV. Effect of temperature on endocytosis and degradation of sulphated proteoglycan by cultured skin fibroblast. J Biosci 1982;4(4):413–8.
[59] Midoux P, Monsigny M. Efficient gene transfer by histidylated polylysine/pDNA complexes. Bioconjug Chem 1999;10(3):406–11.
[60] Mitchell DJ, Kim DT, Steinman L, Fathman CG, Rothbard JB. Polyarginine enters cells more efficiently than other polycationic homopolymers. J Pept Res 2000;56(5):318–25.
[61] Ziegler A. Thermodynamic studies and binding mechanisms of cell-penetrating peptides with lipids and glycosaminoglycans. Adv Drug Deliv Rev 2008;60(4–5):580–97.
[62] Rose GD, Wolfenden R. Hydrogen bonding, hydrophobicity, packing, and protein folding. Annu Rev Biophys Biomol Struct 1993;22:381–415.
[63] Wright LR, Rothbard JB, Wender PA. Guanidinium rich peptide transporters and drug delivery. Curr Protein Pept Sci 2003;4(2):105–24.
[64] Wender PA, Mitchell DJ, Pattabiraman K, Pelkey ET, Steinman L. The design, synthesis, and evaluation of molecules that enable or enhance cellular uptake: peptoid molecular transporters. Proc Natl Acad Sci USA 2000;97(24):13003–8.
[65] Tang M, Waring AJ, Hong M. Phosphate-mediated arginine insertion into lipid membranes and pore formation by a cationic membrane peptide from solid-state NMR. J Am Chem Soc 2007;129(37):11438–46.
[66] Armstrong KM, Baldwin RL. Charged histidine affects alpha-helix stability at all positions in the helix by interacting with the backbone charges. Proc Natl Acad Sci USA 1993;90(23):11337–40.
[67] Manabe E, Sugibayashi K, Morimoto Y. Analysis of skin penetration enhancing effect of drugs by ethanol-water mixed systems with hydrodynamic pore theory. Int J Pharm 1996;129(1–2):211–21.
[68] Goodman M, Barry BW. Action of penetration enhancers on human skin as assessed by the permeation of model drugs 5-fluorouracil and estradiol. I. Infinite dose technique. J Invest Dermatol 1988;91(4):323–7.
[69] Friend DR. Transdermal delivery of contraceptives. Crit Rev Ther Drug Carrier Syst 1990;7(2):149–86.
[70] Bhatia KS, Singh J. Effect of linolenic acid/ethanol or limonene/ethanol and iontophoresis on the in vitro percutaneous absorption of LHRH and ultrastructure of human epidermis. Int J Pharm 1999;180(2):235–50.
[71] Jablonski AE, Kawakami T, Ting AY, Payne CK. Pyrene butyrate leads to cellular binding, not intracellular delivery, of polyarginine-quantum dots. J Phys Chem Lett 2010;1(9):1312–5.